Effect of support on the catalytic activity of manganese oxide catalyts for toluene combustion

Gulin Selda Pozan*

Istanbul University, Faculty of Engineering, Chemical Engineering Department, Avcilar 34320, Istanbul, Turkey

ARTICLE INFO

ABSTRACT

The aim of this work was to study combustion of toluene (1000 ppm) over MnO_2 modified with different supports. α-Al_2O_3 and γ-Al_2O_3 obtained from Boehmite, γ-Al_2O_3 (commercial), SiO_2, TiO_2 and ZrO_2 were used as commercial support materials. In view of potential interest of this process, the influence of support material on the catalytic performance was discussed. The deposition of $9.5MnO_2$ was performed by impregnation over support. The catalysts were characterized by X-ray diffraction (XRD), X-ray photoelectron spectroscopy (XPS), temperature programmed reduction and oxidation (TPR/TPO) and thermogravimetric analysis (TGA). The catalytic tests were carried out at atmospheric pressure in a fixed-bed flow reactor. $9.5MnO_2/\alpha$-Al_2O_3(B) (synthesized from Boehmite) catalyst exhibits the highest catalytic activity, over which the toluene conversion was up to 90% at a temperature of 289 °C. Considering all the characterization and reaction data reported in this study, it was concluded that the manganese state and oxygen species played an important role in the catalytic activity.

© 2012 Elsevier B.V. All rights reserved.

1. Introduction

Volatile organic compounds (VOCs) are not only major contributors to air pollution because of their toxicity, their malodorous, mutagenic, and carcinogenic nature, but also main precursors of ozone and smog formation [1–7]. In many countries, including USA, EU, Japan and Korea, stringent legislations have been passed to abate VOCs emission. It is also recognized that catalytic oxidation is a potential method of controlling emissions of VOCs owing to its low thermal NO_x emissions, low operating cost, and high destructive efficiency [8–10]. At present, the catalysts used for reducing VOC emissions can be divided into two categories: noble metals and metal oxides. The noble metal catalysts such as Pt and Pd [11–16] are generally more active than metal oxides catalysts [17–19]. Although metal oxides have less catalytic activity at low temperatures than the noble metals, they are much cheaper, and allow a higher catalyst loading which leads to a higher active surface area in the metal oxide bed. Thus the metal oxide catalysts are only slightly less active than the noble metals in the oxidation of hydrocarbon [20].

Industrial application of VOC catalytic combustion process involves great volumes of gases. Therefore, it is essential to deposit the catalyst on a structured support to avoid high-pressure drops. The most studied supports are monoliths, which are usually made of ceramic or metal materials, covered with a carrier, alumina, that acts as a support of the active phase [21].

It is widely known that deposition of a metallic oxide on an inert support leads to a catalyst with better catalytic performance compared to the oxide as a bulk catalyst. In part, this is due to the high surface area that supports present. However, from the catalytic behavior point of view, the main reason is the oxide species generated on the surface, which depends on the dispersion of the active phase and its interaction with the support.

In this sense, manganese-based catalysts are cheap, environmentally friendly, and active. Thus they have received increased attention. These catalytic systems generally consist of supported manganese oxides [22–25]. However, Mn-containing mixed oxide systems have gained interest as attractive alternatives due to their increased thermal stability [26–28].

The aim of this work was to study the combustion of toluene (1000 ppm) over MnO_2 modified with different supports (α-Al_2O_3 (from Boehmite), γ-Al_2O_3 (from Boehmite), γ-Al_2O_3, TiO_2, SiO_2 and ZrO_2). In view of potential interest of this process, the influence of support material on the catalytic performance was discussed.

2. Experimental

2.1. Catalyst preparation

Supported manganese oxides were prepared by the impregnation of catalyst supports with the aqueous solution of 0.25 M $Mn(NO_3)_2 \cdot 4H_2O$ (Merck). The MnO_2 loading was 9.5 wt% for all the

* Mobile: +90 532 780 64 21; tel.: +90 212 473 70 70x17789.
  E-mail address: gpozan@istanbul.edu.tr

catalysts. After that catalyst samples were dried at 105 °C for 14 h, and then calcination was carried out at 500 °C in an oven under flowing air for 4 h. The resultant powder was ground at a constant vibration rate of 300 rpm for 15 min in a Retsch MM 200 vibrant-ball mill by using ZrO_2 milling container with 12 mm ZrO_2 milling balls. Particulate size was determined as 53–90 μm. Manganese oxide loading of the catalysts was nominally 9.5 wt%. Support materials were, α-Al_2O_3 (synthesized from Boehmite), γ-Al_2O_3 (synthesized from Boehmite), commercial Al_2O_3 (Merck γ-form), commercial SiO_2 (from Fluka with a surface area of 320 m^2/g (35–75 mesh ASTM)), commercial anatase TiO_2 (purity > 99.99%, Aldrich), ZrO_2 (Merck).

2.2. Preparation of Boehmite

Boehmite was prepared by hydrothermal method in a closed, stainless steel autoclave (Parr 4843) with temperature control. $Al(NO_3)_3 \cdot 9H_2O$ (≥98.5%, Merck) as aluminum salt and NH_3 solution (25 wt.%, Lachema) as precipitating agent were used during the precipitation process. $Al(NO_3)_3 \cdot 9H_2O$ was first dissolved in distilled water to make 5 M solution of Al^{3+} and then NH_3 was added drop by drop to make the pH of the solution 10. The solution was taken into the autoclave for hydrothermal treatment and closed tightly. The contents were heated up to 160 °C and maintained at that temperature for 7 h aging. At the end of the hydrothermal process the product was cooled down to 30–40 °C, filtered and washed with distilled water to remove NO^{3-} anions. The product was dried overnight for 16 h at 105 °C and then calcination was carried out at 300 °C for 2 h. The resultant powder was ground at a constant vibration rate of 300 rpm for 15 min in a Retsch MM 200 vibrant-ball mill by using ZrO_2 milling container with 12 mm ZrO_2 milling balls. Particulate size was determined to be as 53–90 μm.

After prepared Boehmite, calcinations studies were carried out at 500 and 1175 °C in an oven under flowing air for 4 h to convert into γ-Al_2O_3 and α-Al_2O_3 form, respectively. They are labeled as 9.5MnO_2/γ-Al_2O_3(B) and 9.5MnO_2/α-Al_2O_3(B).

2.3. Catalyst characterization

The actual metal content in the catalyst was measured using Thermo Elemental X Series ICP-MS and Varian Spectra Fast Sequential-220 atomic absorption spectrometer with an air acetylene flame.

The surface area was determined by nitrogen adsorption at −196 °C with a Costech sorptometer 1042 equipment. Results were obtained after drying the samples in situ at 200 °C for 4 h.

Thermo gravimetric (TG) analysis was performed using a Shimadzu TGA-60WS thermo gravimetric analyzer. All of the samples were heated from 30 to 1000 °C with a heating rate of 10 °C/min using approximately 15 mg of sample powder under flowing air (50 ml/min). The decomposition behavior and weight loss steps were observed in TG curves.

Powder X-ray diffractions of samples were obtained on a Rigaku D/Max-2200 diffractometer by using the Cu Kα (λ = 1.5405) radiation. Samples were scanned from 10 to 80 at a rate of 0.5°/min (in 2θ). The sizes of the crystalline domains were calculated by using the Scherrer equation, $t = C\lambda / B\cos\theta$, where λ is the X-ray wavelength (Å), B is the full width at half maximum, θ is Bragg angle, C is a factor depending on crystallite shape (taken to be one), and t is the crystallite size (Å). By using Xpowder program, line broadening has been taken into account. The variation of the FWHM of the peaks is generally described by the Caglioti equation, values found after such correction were calculated and tabulated in.

The morphology and size distribution of the catalysts were recorded by scanning electron microscopy (JEOL/JSM-6335F).

The X-ray photoelectron spectroscopy (XPS) was performed on the SPECS EA 300 with an Al monochromatic anode.

Temperature programmed reduction (TPR) was performed to monitor the reduction of the metal oxide while the temperature increased from 60 to 600 °C. TPR profiles were obtained by using Quantachrome ChemBET 3000 flow type equipment. In TPR experiments, 60 mg of the catalyst was dried at 105 °C for 2 h, and 10% H_2/N_2 (BOS, 99.99% purity) was used as a reducing gas. Temperature ramp rate was 10 °C/min and flow rate was 70 ml/min. The changes in H_2 flow were followed using a thermal conductivity detector.

Recording successive reduction/oxidation cycles helped in monitoring the compositional stability during the prolonged use of a catalyst. TPO profile was obtained by using Quantachrome ChemBET 3000 flow type equipment. After TPR experiments, the reduced sample were oxidized using air with a flow rate of 70 ml/min, increasing the temperature from room temperature to 600 °C at a heating rate of 10 °C/min.

2.4. Catalytic evaluation

Catalytic activity was determined using a fixed-bed reactor, in which typically 0.15 g of powder catalyst was loaded between glass wool packings. Prior to catalytic tests, catalyst precursors were heated in a flowing air up to 500 °C at the rate of 10 °C/min, and annealed at this temperature for 1 h. Catalytic activity of the calcined samples was measured in total combustion of toluene in air. The reaction feed consisted of 1000 ppm of toluene together with a dry air as the balance. The feed stream to the reactor was prepared by delivering toluene by a syringe pump (Cole Palmer 74900-05) into dry air, which was metered by a mass flow controller (Brooks, 5850TR). A total flow rate of 500 cm^3 min^{-1} was used and catalysts were packed to a constant volume to give a gas hourly space velocity of 15,000 h^{-1} for all studies. Catalytic activity was measured over the range of 150–550 °C, and temperatures were measured by a thermocouple placed in the catalyst bed. Conversion data were calculated by the difference between inlet and outlet concentrations. Conversion measurements and product profiles were taken at steady state, typically after 30 min on stream. The feed and the reaction products were analyzed by on-line gas chromatography (HP 6890+) equipped with a thermal conductivity detector (TCD) and a flame ionization detector (FID) in series. The hydrocarbons and carbon dioxide were analyzed with a Poraplot Q capillary column (30 m × 0.530 mm × 40 μm) and carbon monoxide with a Molecular Sieve 5A capillary column (30 m × 0.530 mm × 50 μm), both columns being connected in parallel.

3. Results and discussion

3.1. Structure and texture properties

The boehmite did not contain $Al(OH)_3$ phase after the hydrothermal synthesis. It was also confirmed by the thermogravimetric (TG) and X-ray diffraction analyses. Thermogravimetric analysis (TGA) was carried out to explore the thermal behavior of boehmite sample. The TG–DTG curves of boehmite are shown in Fig. 1a. The slight weight loss at below 150 °C was caused by the removal of the adsorbed water. Noticeable weight loss seen between 400 and 510 °C could be ascribed to the decomposition of the boehmite to the γ-Al_2O_3 phase [29,30]. The transform process of boehmite AlOOH to γ-Al_2O_3 involves the elimination of hydrogen bonds from boehmite [31]. Temperature of phase transition into γ-Al_2O_3 is lower than the standard value of 550 °C [29].

The BET surface areas of supports and supported manganese oxide catalysts were measured, and listed in Table 1. The BET surface of the fresh α-Al_2O_3 support is 32 m^2/g. However, the specific

Table 1
Metal oxide content, crystallite size of catalysts, BET surface area, and H and O consumption values of catalysts in TPR/TPO analysis.

Catalyst	Metal oxide content (wt%)	Crystallite size (nm)	BET surface area (m^2/g)		mmol H$_2$/g$_{cat}$	mmol O$_2$/g$_{cat}$
	Experimental		Fresh	After impregnation		
9.5MnO$_2$/α-Al$_2$O$_3$(B)	9.43	70	37	15	0.526	0.256
9.5MnO$_2$/γ-Al$_2$O$_3$(B)	9.40	32	179	141	0.384	0.152
9.5MnO$_2$/γ-Al$_2$O$_3$	9.41	37	172	110	0.362	0.137
9.5MnO$_2$/ZrO$_2$	9.40	28	45	21	0.413	0.189
9.5MnO$_2$/TiO$_2$	9.42	37	46	27	0.428	0.147
9.5MnO$_2$/SiO$_2$	9.39	33	320	280	0.345	0.130

surface area of γ-Al$_2$O$_3$ and γ-Al$_2$O$_3$(B) are 172 and 179 m^2/g, respectively. On the other hand, after impregnation, BET surface areas of the catalysts decreased. This effect may be attributed to the result of some pore blockage after the manganese oxide impregnation. Comparing to that of pure SiO$_2$ support, the surface area of the supported Mn catalyst decreased 12%. The manganese oxide's better dispersion over SiO$_2$ resulted in relatively higher surface area. Consequently, the metallic dispersion of 9.5MnO$_2$/α-Al$_2$O$_3$ appeared to be poorer compared with 9.5MnO$_2$/SiO$_2$ catalyst. Although the decrease in surface area of 9.5MnO$_2$/α-Al$_2$O$_3$ catalyst was comparable even lower than 9.5MnO$_2$/SiO$_2$, it showed high activity. However, the changes in surface areas were not as drastic as the changes in catalytic activities. Hence, the activity comparisons were due to the active species on the surface.

In a similar way, Kim et al. have examined iron-based spent catalysts (89 wt% Fe$_2$O$_3$, 9 wt% Cr$_2$O$_3$ and balance Al$_2$O$_3$) on the catalytic oxidation of toluene. However, the BET surface area of the catalyst showed low surface area (13 m^2/g). The conversion of toluene to CO$_2$ was 50% at 265 °C [32].

It is said that surface areas of the catalysts seemed to control the activities of the catalysts. As a result, it was observed with a corresponding trend in activity as listed in Tables 1 and 2. It is clearly seen that the catalytic activity of the catalysts increased with a decrease in the surface area. As is known, toluene is quite large molecule compared with a water molecule. Adsorbing larger molecules on low surface area adsorbents allow them to be thermally desorbed more easily. In addition, it reduces the risk of thermal degradation. For example, carbon adsorbents with large surface areas (ca 100 m^2/g) are used for adsorbing small molecular weight materials. Adsorbents with low surface areas (ca 5 m^2/g) are suitable for adsorbing large molecules [33].

The boehmite was characterized by powder X-ray diffraction for their crystalline nature (Fig. 1b). All the sharp reflection peaks can be assigned as aluminium oxide hydroxide (AlO(OH), JCPDS 49-0133) with high crystallinity.
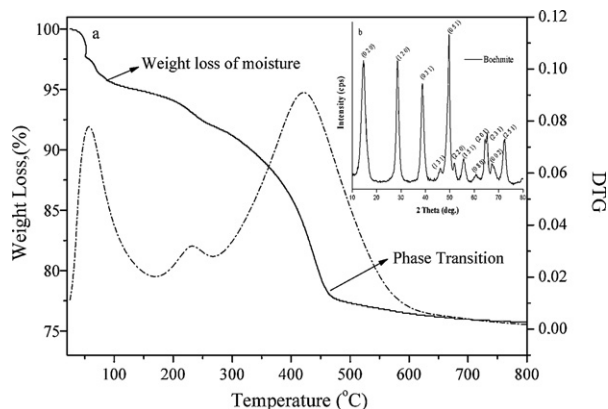
Theoretical and experimental manganese content values are shown in Table 1. The values determined experimentally are in reasonable agreement with the theoretical values.

The dispersion and the state of manganese species on different supports were investigated by X-ray diffraction studies. Diffraction patterns of manganese oxide phase were observed for the catalysts. XRD patterns match the diffraction pattern of crystalline tetragonal MnO$_2$ (JCPS 44-0141).

Support influence was not observed for the diffractograms of the supported manganese catalysts, but the crystallinity was very different depending on the support. Crystallite sizes of manganese oxides supported on different support at loading level of 9.5 wt% were calculated and listed in Table 1.

The morphologies of the supported manganese catalysts were analyzed by SEM. Selected SEM images of 9.5MnO$_2$/γ-Al$_2$O$_3$, 9.5MnO$_2$/γ-Al$_2$O$_3$(B) and 9.5MnO$_2$/α-Al$_2$O$_3$(B) are compared in Fig. 2a–c, respectively. The morphology of 9.5MnO$_2$/α-Al$_2$O$_3$(B) is different from 9.5MnO$_2$/γ-Al$_2$O$_3$ and 9.5MnO$_2$/γ-Al$_2$O$_3$(B).

It can be observed that aggregated MnO$_2$ particles, which exhibit an irregular shape settle on the outside surface of γ-Al$_2$O$_3$ and support for 9.5MnO$_2$/γ-Al$_2$O$_3$ while the image of 9.5MnO$_2$/α-Al$_2$O$_3$(B) features a number of MnO$_2$ particles on the surface of α-Al$_2$O$_3$(B). However, the morphology of 9.5MnO$_2$/γ-Al$_2$O$_3$(B) is different from 9.5MnO$_2$/γ-Al$_2$O$_3$. The primary particles exhibit regular shapes and distribution. Meanwhile, leaf-like MnO$_2$ particles grew on the γ-Al$_2$O$_3$(B) support.

The amount of coke over used catalysts was also measured from the weight losses of samples recorded under flowing air in TGA. In pyrolysis run, coke and catalysts were remained, however only catalysts remained in the thermal degradation run under oxidative conditions (air atmosphere). As seen in Fig. 3, it is observed that the weight losses of calcined and used catalysts were almost zero for 9.5MnO$_2$/α-Al$_2$O$_3$(B) catalyst. It confirmed no coke formation occurred during total combustion of toluene over 9.5MnO$_2$/α-Al$_2$O$_3$(B).

3.2. Surface properties of supported Mn catalysts

The XPS spectra of Mn 2p and O 1s were measured for these five supported Mn catalysts are presented in Figs. 4 and 5. The results of XPS measurements are listed in Table 3. According to Fig. 4, the XPS spectrum has a larger doublet separation of Mn 2p$_{1/2}$ and Mn 2p$_{3/2}$ spin orbit levels. The binding energies of Mn 2p$_{3/2}$ (641.9–640.5 eV) could be ascribed to Mn^{4+} species [34], in good agreement with the XRD results. In addition, Zimowska et al. [35] have characterized the surface composition of the calcined CuMn(x) mixed oxides by means of the XPS spectroscopy. Two major components were obtained with the binding energies of 642.2 eV and 640.7 eV. The results correspond closely to the values reported for Mn^{4+} and Mn^{2+} [36]. According to the XPS spectra of O 1s, two peaks (O$_I$ and O$_{II}$) were displayed, which represented two different kinds of surface oxygen species. O$_I$ with binding energy from 528.5 to 528.7 eV was characteristic of the lattice oxygen (O^{2-}) [37], while O$_{II}$ with binding energy of 530.1–530.7 eV belonged

Fig. 1. TG–DTG curves of bohmite. Inset shows the XRD pattern of boehmite.

Table 2
T_{10}, T_{50} and T_{90} values and ignition temperature at maximum conversion to CO_2.

Catalyst	Catalytic activity			T (°C) (CO_2 (max)%)
	T_{10} (°C)	T_{50} (°C)	T_{90} (°C)	
$9.5MnO_2/\alpha$-Al_2O_3(B)	162	213	289	350 (100)
$9.5MnO_2/\gamma$-Al_2O_3(B)	260	–	–	550 (49)
$9.5MnO_2/\gamma$-Al_2O_3	297	–	–	550 (42)
$9.5MnO_2/ZrO_2$	260	328	–	550 (92)
$9.5MnO_2/TiO_2$	271	–	–	550 (60)
$9.5MnO_2/SiO_2$	399	–	–	550 (13)
MnO_2	267	329	441	550 (100)

probably to the surface oxygen ions with low coordination [38]. Combining XPS data with the values in Table 3, more lattice oxygen was observed on $9.5MnO_2/\alpha$-Al_2O_3(B) compared to $9.5MnO_2/\gamma$-Al_2O_3 and $9.5MnO_2/SiO_2$ and more surface oxygen compared to $9.5MnO_2/TiO_2$ and $9.5MnO_2/ZrO_2$. There were only surface oxygen O_{II} presented on $9.5MnO_2/\gamma$-Al_2O_3 and $9.5MnO_2/SiO_2$.

3.3. Temperature-programmed reduction (TPR) and oxidation (TPO) measurements

The reducibility of Mn sites in different supports was studied by H_2-TPR. These measurements were carried out on manganese oxide supported and calcined catalysts, and allowed us to calculate the quantity of hydrogen consumed and estimate the reducibility of manganese oxide species, which depended on the interactions with exchanged support. In addition, TPR analyses of catalysts are well correlated with the conclusion in the crystallographic and morphological studies.

The TPR profiles of the supported manganese oxide are presented in Fig. 6. The supported MnO_2 catalysts showed a two-step reduction process [39,40]:

$$MnO_2 \rightarrow Mn_3O_4 \rightarrow MnO.$$
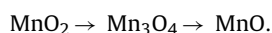
The reduction behaviors of the catalysts were influenced by support material. Compared to the reduction behaviors of $9.5MnO_2/\alpha$-Al_2O_3(B), $9.5MnO_2/\gamma$-Al_2O_3(B), $9.5MnO_2/\gamma$-Al_2O_3, $9.5MnO_2/TiO_2$, $9.5MnO_2/SiO_2$ and $9.5MnO_2/ZrO_2$ catalysts exhibited lower reduction temperature in the first reduction steps. It was observed from Fig. 6 that the reduction temperature values of $9.5MnO_2/\gamma$-Al_2O_3 and $9.5MnO_2/\gamma$-Al_2O_3(B) catalysts were close to each other.

The TPR profile of $9.5MnO_2/\alpha$-Al_2O_3(B) showed two broad peaks at about 392 and 463 °C. However, a shift of the TPR peaks to lower temperatures was observed with the sample supported by $9.5MnO_2/\gamma$-Al_2O_3. The two reduction peaks were decreased to 341 °C and 434 °C for $9.5MnO_2/\gamma$-Al_2O_3. In addition, the first peak was decreased to 337 °C over $9.5MnO_2/\gamma$-Al_2O_3(B) catalyst. The decrease of reduction temperature indicated the easier reduction of manganese oxide. It may be noted that the first reduction peak also shifted to higher temperature for $9.5MnO_2/\alpha$-Al_2O_3(B). This was caused by the increase in the number of manganese oxide layers dispersed on α-Al_2O_3(B) surface [41]. Therefore, the sample $9.5MnO_2/\alpha$-Al_2O_3(B) exhibited the largest hydrogen and oxygen consumption.

A close examination of TPR profiles reveals that maximum reduction temperatures of these catalysts were changing. As a conclusion, the support does not only change the structure and the reductivity of MnO_2 species.

From Table 1, it can be concluded that the largest crystallite sizes of MnO_2 was obtained for $9.5MnO_2/\alpha$-Al_2O_3(B). Results from XRD and TPR of $9.5MnO_2/\alpha$-Al_2O_3(B) catalyst revealed the presence of relatively large crystal of MnO_2 specie which required higher temperature for complete reduction [39].

The reoxidation of reduced catalysts was studied by temperature programmed oxidation, TPO. The results from TPO experiment are listed in Table 1. TPO profile showed that the temperatures, where oxidation was occurred, were in line with TPR profile. TPO profile of $9.5MnO_2/\alpha$-Al_2O_3(B) catalyst showed two peaks at 364 and 446 °C representing oxygen consumption during the process. The result showed that the stepwise backward oxidation of metallic MnO to MnO_2 occurred. However, the oxidation temperatures decreased and also shifted to lower temperature after reduction process. When O_2 consumption values of catalysts were considered, it was observed that reduced $9.5MnO_2/\alpha$-Al_2O_3(B) catalyst has consumed O_2 at a value that is half of hydrogen consumption value. In a similar context, De Rivas et al. prepared ceria-zirconia mixed oxides and evaluated the oxygen storage capacity of the catalysts. It was found that the reducibility (1.32 mmol H_2 g^{-1}) reached a maximum for the $Ce_{0.5}Zr_{0.5}O_2$ sample, which exhibited an oxygen storage capacity value of approximately 0.45 mmol O_2 g^{-1} [42].

According to TPR and TPO results, the $9.5MnO_2/\alpha$-Al_2O_3(B) catalyst was better in reduction/oxidation cycle than the other catalysts. The increase in catalytic activity was essentially assigned to the oxygen excess at the catalyst surface.

3.4. Catalyst performance for toluene catalytic combustion

The oxidation activity was recorded by following the evolution of conversion with temperature (the so-called light-off curves). The selectivity towards CO_2 was almost 100% and no intermediates, such as CO or other hydrocarbons, were detected. The decomposition of toluene started above 150 °C.

The bare α-Al_2O_3, γ-Al_2O_3, SiO_2, TiO_2 and ZrO_2 supports were shown to be completely inactive for this oxidation reaction. In literature, diverse supports (Al_2O_3, SiO_2, TiO_2 and ZrO_2) have been reported [43–45].
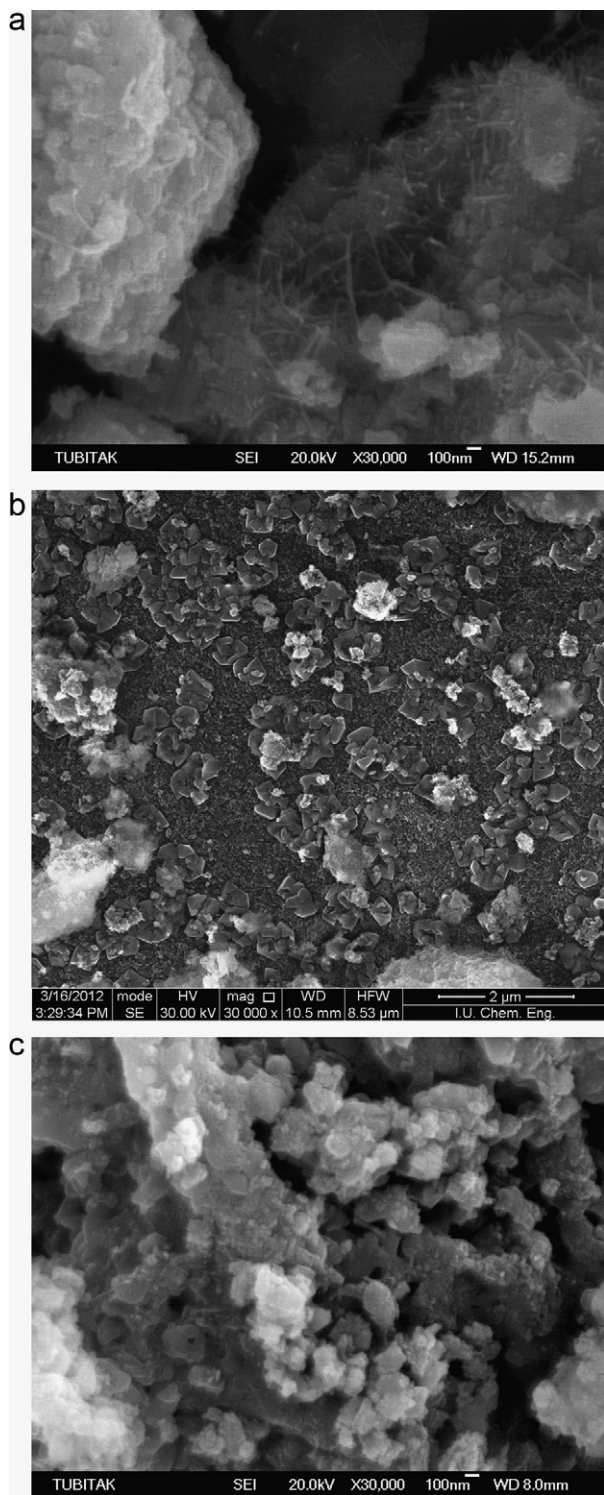
Table 3
XPS results of supported Mn-based catalysts.

Catalyst	Binding energy of Mn $2p_{3/2}$ (eV)	Binding energy (eV)		$O_I/(O_I + O_{II})$ (%)	$O_{II}/(O_I + O_{II})$ (%)
		O_I	O_{II}		
$9.5Mn/\alpha$-Al_2O_3(B)	640.5	528.7	530.7	41.8	58.2
$9.5Mn/\gamma$-Al_2O_3	641.5	–	530.1	0	100
$9.5Mn/TiO_2$	640.9	528.5	530.4	78.5	21.5
$9.5Mn/ZrO_2$	640.5	528.6	530.7	82.2	17.8
$9.5Mn/SiO_2$	641.9	–	530.3	0	100

Fig. 2. SEM images of (a) $9.5MnO_2/\gamma\text{-}Al_2O_3$, (b) $9.5MnO_2/\gamma\text{-}Al_2O_3(B)$, and (c) $9.5MnO_2/\alpha\text{-}Al_2O_3$ (B).

Fig. 3. The weight losses of calcined and used $9.5MnO_2/\alpha\text{-}Al_2O_3(B)$ catalyst.
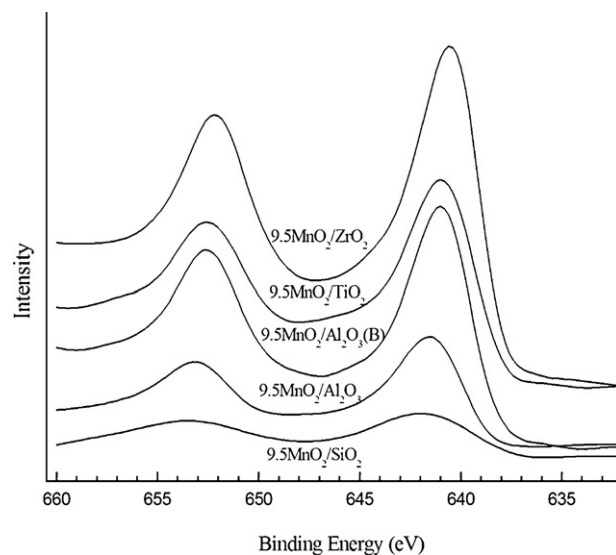
Fig. 4. XPS spectra of Mn 2p for various catalyts.
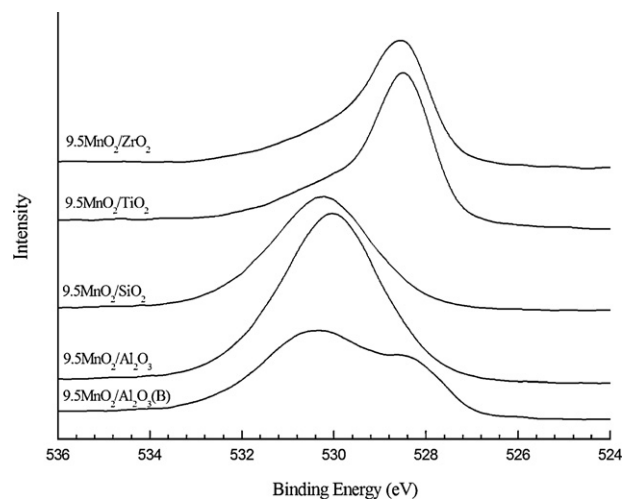
Fig. 5. XPS spectra of O 1s for various catalyts.

In our previous study, it was reported [46] that manganese oxide exhibited higher catalytic activity for the low-temperature catalytic combustion of toluene than other oxides. $9.5MnO_2/NaCLT$ catalyst showed the catalytic conversion of toluene to 93% at a temperature of 350 °C. However, increasing combustion temperature above 350 °C led to major decrease in activity due to the interaction between the exchanged ion and the zeolite. In addition to this study, different supported MnO_x catalyst (9.5 wt% Mn loading) was
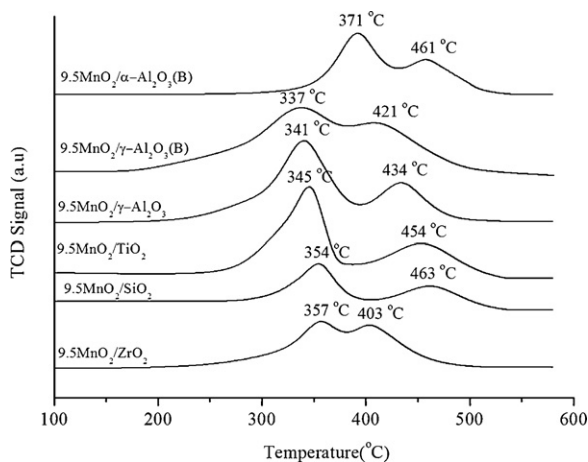
Fig. 6. TPR patterns of various supported manganese oxide catalysts.

performed and it was observed that favorable higher activity and considerable lowering in T_{50} and T_{90} temperatures were obtained by adding manganese nitrate to boehmite and better manganese oxide stabilization on the alumina support was reached after calcination.

Catalytic combustion of toluene over different supported MnO_x catalyst (9.5 wt% Mn loading) is shown in Fig. 7. As shown in Fig. 7, manganese oxide supported on α-Al_2O_3 (from Boehmite) was found more active for toluene combustion, over which conversion of toluene reached 100% at 450 °C. It was observed that T_{90} values were obtained for $9.5MnO_2/\alpha$-Al_2O_3. Furthermore, 100% conversion of toluene was obtained with these catalysts.

The $9.5MnO_2/\alpha$-Al_2O_3 catalyst exhibits the highest catalytic activity over which the toluene conversion is up to 50% at a temperature of 213 °C. T_{90}, which is the temperature where 90% conversion of toluene was obtained, was reached at 289 °C. These experiments were also carried out over a $9.5MnO_2$ loaded on commercial catalysts for comparison purpose. T_{90} values were not obtained under the conditions studied here. But, for the only $9.5MnO_2/ZrO_2$ catalyst, 50% conversion of toluene was achieved. T_{10}, T_{50}, T_{90} and maximum CO_2 conversion temperatures were shown in Table 2. It can be seen that the activity of $9.5MnO_2/\alpha$-Al_2O_3(B) highly exceeded compared with $9.5MnO_2/\gamma$-Al_2O_3 for toluene combustion. Besides, $9.5MnO_2/\gamma$-Al_2O_3(B) was found more active than $9.5MnO_2/\gamma$-Al_2O_3. In addition, a blank reactor
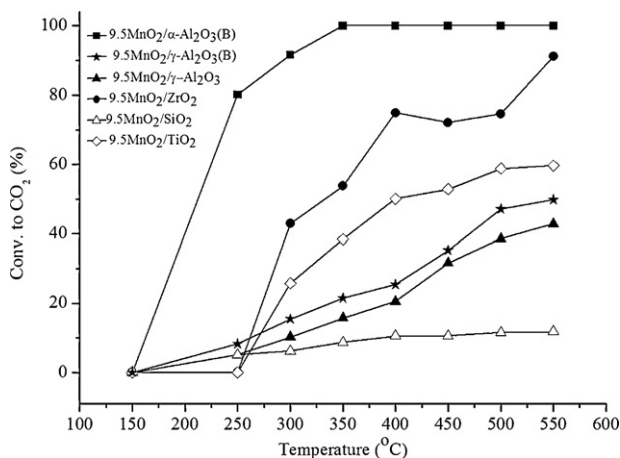
experiment (homogeneous reaction) indicated no significant gas-phase oxidation of toluene at 550 °C.

$9.5MnO_2/\gamma$-Al_2O_3 and $9.5MnO_2/SiO_2$ had more surface oxygen than the other three samples, which assures that it was more active at low temperature values, but no lattice oxygen resulted in its poor activity at high temperature values. According to the reference [47], the Mn oxidation state changed from Mn^{4+} to Mn^{2+} in oxidation reaction, by providing oxygen to the reactants, and thus leading to the formation of the less active Mn_3O_4 species. The formation of Mn_3O_4 might be responsible for the decrease in the catalytic activity of the $9.5MnO_2/\gamma$-Al_2O_3 and $9.5MnO_2/SiO_2$ catalysts.

4. Conclusion

Amongst the MnO_2-based catalysts supported on α-Al_2O_3 (from Boehmite), γ-Al_2O_3 (from Bohmite),γ-Al_2O_3, SiO_2, TiO_2, and ZrO_2, (Mn/α-Al_2O_3) presented better catalytic performance for the combustion of toluene. Mn/α-Al_2O_3 catalyst with 9.5%Mn loading had a high activity and toluene conversion of 90% which was obtained at a low temperature of 289 °C. Considering all the characterization and reaction data reported in this study, it is concluded that support surfaces affected surface active MnO_2 species. The lattice oxygen and surface oxygen species are effective for catalytic combustion of toluene.

α-Al_2O_3 (from Boehmite) type support not only facilitated the combustion and also lowered light-off temperature too. Manganese oxides impregnated α-Al_2O_3 support showed unusually high catalytic combustion activity for the commercial catalysts reported in open literature.

Acknowledgements

References

[1] K. Everaert, J. Baeyens, Catalytic combustion of volatile organic compounds, J. Hazard. Mater. B 109 (2004) 113–139.
[2] K. Everaert, M. Mathieu, J. Baeyens, E.V. Vansant, Combustion of chlorinated hydrocarbons in catalyst-coated sintered metal fleece reactors, J. Chem. Technol. Biotechnol. 78 (2003) 167–172.
[3] M. Alifanti, M. Florea, S. Somacescu, V.I. Parvulescu, Supported perovskites for total oxidation of toluene, Appl. Catal. B: Environ. 60 (2005) 33–39.
[4] H.L. Tidahy, S. Siffert, F. Wyrwalski, J.F. Lamonier, A. Aboukäis, Catalytic activity of copper and palladium based catalysts for toluene total oxidation, Catal. Today 119 (2007) 317–320.
[5] R. Dula, R. Janik, T. Machej, J. Stoch, R. Grabowski, E.M. Serwicka, Mn-containing catalytic materials for the total combustion of toluene: the role of Mn localisation in the structure of LDH precursor, Catal. Today 119 (2007) 327–331.
[6] M.F. Ribeiro, J.M. Silva, S. Brimaud, A.P. Antunes, E.R. Silva, A. Fernandes, P. Magnoux, D.M. Murphy, Improvement of toluene catalytic combustion by addition of cesium in copper exchanged zeolites, Appl. Catal. B: Environ. 70 (2007) 384–392.
[7] S.K. Ihm, Y.D. Jun, D.C. Kim, K.E. Jeong, Low temperature deactivation and oxidation state of Pd/γ-Al2O3 catalysts for total oxidation of n-hexane, Catal. Today 93 (95) (2004) 149–154.
[8] J.J. Spivey, Complete catalytic oxidation of volatile organics, Ind. Eng. Chem. Res. 26 (1987) 2165–2180.
[9] D.R. Van der Vaart, M.W. Vatavuk, A.H. Wehe, Thermal and catalytic incinerators for the control of VOCs, J. Air Waste Manage. Assoc. 41 (1991) 92–98.
[10] D.R. Van der Vaart, M.W. Vatavuk, A.H. Wehe, The cost estimation of thermal and catalytic incinerators for the control of VOCs, J. Air Waste Manage. Assoc. 41 (1991) 497–501.
[11] T. Garcia, B. Solsona, D.M. Murphy, K.L. Antcliff, S.H. Taylor, Deep oxidation of light alkanes over titania-supported palladium/vanadium catalysts, J. Catal. 229 (2005) 1–11.
[12] E.M. Cordi, J.L. Falconer, Oxidation of volatile organic compounds on Al2O3, Pd/Al2O3, and PdO/Al2O3 catalysts, J. Catal. 162 (1996) 104–117.
[13] J.C.S. Wu, Z.A. Lin, F.M. Tsai, J.W. Pan, Low-temperature complete oxidation of BTX on Pt/activated carbon catalysts, Catal. Today 63 (2000) 419–426.
[14] J. Tsou, P. Magnoux, M. Guisnet, J.J.M. Orfao, J.L. Figueiredo, Catalytic oxidation of volatile organic compounds: oxidation of methyl-isobutyl-ketone over Pt/zeolite catalysts, Appl. Catal. B: Environ. 57 (2005) 117–123.

Fig. 7. Light-off curves of combustion of toluene vs. reaction temperature over different catalysts.

[15] P. Dege, L. Pinard, P. Magnoux, M. Guisnet, Catalytic oxidation of volatile organic compounds (VOCs). Oxidation of o-xylene over Pd and Pt/HFAU catalysts, Surf. Chem. Catal. 4 (2001) 41–47.

[16] B. Grbic, N. Radic, A. Terlecki-Baricevic, Kinetics of deep oxidation of n-hexane and toluene over Pt/Al$_2$O$_3$ catalysts: oxidation of mixture, Appl. Catal. B: Environ. 50 (2004) 161–166.

[17] E.M. Cordi, P.J. O'Neill, J.L. Falconer, Transient oxidation of volatile organic compounds on a CuO/Al$_2$O$_3$ catalyst, Appl. Catal. B: Environ. 14 (1997) 23–36.

[18] S.C. Kim, The catalytic oxidation of aromatic hydrocarbons over supported metal oxide, J. Hazard. Mater. B 91 (2002) 285–299.

[19] C.H. Wang, S.S. Lin, C.L. Chen, H.S. Weng, Performance of the supported copper oxide catalysts for the catalytic incineration of aromatic hydrocarbons, Chemosphere 64 (2006) 503–509.

[20] C.H. Wang, Al$_2$O$_3$-supported transition-metal oxide catalysts for catalytic incineration of toluene, Chemosphere 55 (2004) 11–17.

[21] P. Avila, M. Montes, E. Miró, Monolithic reactors for environmental applications: a review on preparation technologies, Chem. Eng. J. 109 (2005) 11–36.

[22] C. Lahousse, A. Bernier, P. Grange, B. Delmon, P. Papaefthimiou, T. Ioannides, X. Verykios, Evaluation of γ-MnO$_2$ as a VOC removal catalyst: comparison with a noble metal catalyst, J. Catal. 178 (1998) 214–225.

[23] K. Poplawski, J. Lichtenberger, F.J. Keil, K. Schnitzlein, M.D. Amiridis, Catalytic oxidation of 1,2-dichlorobenzene over ABO3-type perovskite, Catal. Today 62 (2000) 329–336.

[24] J.I. Gutiérrez-Ortiz, R. López-Fonseca, U. Aurrekoetxea, J.R. González-Velasco, Low-temperature deep oxidation of dichloromethane and trichloroethylene by H-ZSM-5-supported manganese oxide catalysts, J. Catal. 210 (2001) 148–154.

[25] C. Cellier, V. Ruaux, C. Lahousse, P. Grange, E.M. Gaigneaux, Extent of the participation of lattice oxygen from γ-MnO$_2$ in VOCs total oxidation: influence of the VOCs nature, Catal. Today 117 (2006) 350–355.

[26] Y. Liu, M. Luo, Z. Wei, Q. Xin, P. Ying, C. Li, Catalytic oxidation of chlorobenzene on supported manganese oxide catalysts, Appl. Catal. B: Environ. 29 (2000) 61–67.

[27] E. Fernández-López, V. Sánchez-Escribano, C. Resini, J.M. Gallardo-Amores, G. Busca, A study of coprecipitated Mn–Zr oxides and their behavior as oxidation catalysts, Appl. Catal. B: Environ. 29 (2001) 251–261.

[28] D. Döbber, D. Kießling, W. Schmitz, G. Wendt, MnO$_x$/ZrO$_2$ catalysts for the total oxidation of methane and chloromethane, Appl. Catal. B: Environ. 52 (2004) 135–143.

[29] Y. Li, J. Liu, Z. Jia, Fabrication of boehmite AlOOH nanofibers by a simple hydrothermal process, Mater. Lett. 60 (2006) 3586–3590.

[30] M. Inoue, M. Kimura, T. Inui, Alkoxyalumoxanes, Chem. Mater. 12 (2000) 55.

[31] X.Y. Chena, Z.J. Zhangb, X.L. Li, S.W. Lee, Controlled hydrothermal synthesis of colloidal boehmite (γ-AlOOH) nanorods and nanoflakes and their conversion into γ-Al$_2$O$_3$ nanocrystals, Solid State Commun. 145 (2008) 368–373;
D. Mishra, S. Anand, R.K. Panda, R.P. Das, Hydrothermal preparation and characterization of boehmites, Mater. Lett. 42 (2000) 38–45.

[32] S.C. Kim, W.G. Shim, Influence of physicochemical treatments on iron-based spent catalysts for catalytic oxidation of toluene, J. Hazard. Mater. 154 (2008) 310–316.

[33] T.E. Beesley, B. Buglio, R.P.W. Scott, Sample collection, transport and storage, in: New Quantitative Chromatographic Analysis, Marcel Dekker, Inc., New York, 2001, pp. 13–33.

[34] M. Ferrandon, J. Carnö, S. Jaras, E. Björnbom, Total oxidation catalysts based on manganese or copper oxides and platinum or palladium. I. Characterisation, Appl. Catal. A 180 (1–2) (1999) 141–151.

[35] M. Zimowska, A. Michalik-Zym, R. Janik, T. Machej, J. Gurgul, R.P. Socha, J. Podobínski, E.M. Serwicka, Catalytic combustion of toluene over mixed Cu–Mn oxides, Catal. Today 119 (2007) 321–326.

[36] B. Gillot, S. Buguet, E. Kester, C. Baubet, Ph. Tailhades, Thin Solid Films 357 (1999) 223.

[37] H. Chen, A. Sayari, A. Adnot, F.V. Larachi, Composition–activity effects of Mn–Ce–O composites on phenol catalytic wet oxidation, Appl. Catal. B: Environ. 32 (3) (2001) 195–204.

[38] X.F. Tang, Y.G. Li, X.M. Huang, Y.D. Xu, H.Q. Zhu, J.G. Wang, W. Shen, MnO$_x$–CeO$_2$ mixed oxide catalysts for complete oxidation of formaldehyde: effect of preparation method and calcination temperature, Appl. Catal. B 62 (3–4) (2006) 265–273.

[39] J.I. Gutiérrez-Ortiz, R. López-Fonseca, U. Aurrekoetxea, J.R. Gonzalez-Velasco, Low-temperature deep oxidation of dichloromethane and trichloroethylene by H-ZSM-5-supported manganese oxide catalysts, J. Catal. 218 (2003) 148–154.

[40] M.F. Luo, X.X. Yuan, X.M. Zheng, Catalyst characterization and activity of Ag–Mn, Ag–Co and Ag–Ce composite oxides for oxidation of volatile organic compounds, Appl. Catal. A 175 (1–2) (1998) 121–129.

[41] M.C. Alvarez-Galvan, V.A. denla Pena O'Shena, J.L.G. Fierro, P.L. Arias, Alumina-supported manganese-and manganese-palladium oxide catalysts for VOCs combustion, Catal. Commun. 4 (2003) 223–228.

[42] B. de Rivas, J.I. Gutiérrez-Ortiz, R. López-Fonseca, J.R. González-Velasco, Analysis of the simultaneous catalytic combustion of chlorinated aliphatic pollutants and toluene over ceria-zirconia mixed oxides, Appl. Catal. A 314 (2006) 54–63.

[43] S. Yuan, P. Meriaıdeau, V. Perrichon, Catalytic combustion of diesel soot particles on copper catalysts supported on TiO$_2$. Effect of potassium promoter on the activity, Appl. Catal. 3 (1994) 319–333.

[44] J. van Doorn, J. Varloud, P. Mériaudeau, V. Perrichon, M. Chevrier, C. Gauthier, Effect of support material on the catalytic combustion of diesel soot particulates, Appl. Catal. B 1 (1992) 117–127.

[45] A. Carrascull, C. Grzona, I.D. Lick, M. Ponzi, E. Ponzi, SOOT combustion. Co and K catalysts supported on different supports, React. Kinet. Catal. Lett. 75 (2002) 63–68.

[46] Z. Özçelik, G.S. Pozan Soylu, I. Boz, Catalytic combustion of toluene over Mn, Fe and Co-exchanged clinoptilolite support, Chem. Eng. J. 155 (2009) 94–100.

[47] R. Craciun, Structure/activity correlation for unpromoted and CeO$_2$-promoted MnO$_2$/SiO$_2$ catalysts, Catal. Lett. 55 (1) (1998) 25–31.